Onset of neutron single-particle strengths in the tin isotopic chain

C. P. Massolo,* S. Fortier, S. Galès, F. Azaiez,† E. Gerlic,‡ J. Guillot,
E. Hourani, H. Langevin-Joliot, J. M. Maison, and J. P. Schapira
Institut de Physique Nucleaire, 91406 Orsay CEDEX, France

G. M. Crawley
National Superconducting Cyclotron Laboratory, Michigan State University, East Lansing, Michigan 48824
(Received 18 July 1990)

The stripping reaction $(\alpha,{}^3\mathrm{He})$ at 183 MeV bombarding energy has been used to study the neutron-particle response function on ^{124,122,120,118,116,112}Sn target nuclei up to 25 MeV excitation energy. Strong transitions to high-lying neutron states are observed beyond 4 MeV excitation energy. These transitions, arising from neutron stripping to high-spin outer subshells, appear as a sharp and strong peak located around 5 MeV excitation energy for the heavier tin isotopes (125, 123, and 121) and a broader structure extending up to 10 MeV. A clear broadening of the whole structure and the disappearance of the sharp component is observed with decreasing mass number, leading to a structureless spectrum in the case of ^{113}Sn. Our investigation reveals a strong excitation of the $1i_{13/2}$ neutron strength, with possible mixture with the neighboring $1h_{9/2}$ and $2f$ subshells between 5 and 10 MeV excitation energy. The empirical data are compared with the theoretical predictions from the quasiparticle-phonon nuclear model. The present investigation, on a wide range of the tin isotopic chain, allows us to establish a comparison between the damping of high-lying particle and deep-hole states in heavy nuclei.

I. INTRODUCTION

Due to the closure of the proton shell ($Z=50$) and to the large number of even-even stable isotopes, the tin isotopes have been the subject of a large number of experiments on inner neutron-hole strength distributions.[1] The investigations using neutron pick-up reactions revealed cross-section enhancements around 5, 7, and 15 MeV excitation energy, which have been attributed to the pick-up of a neutron from the next lower shell, e.g., the $1g_{9/2}$, $2p$, and $1f$ subshells.[2–9] It has been shown that a large fraction of $1f_{5/2}$ strength is located at high excitation energy[8,9] (around 8 to 12 MeV in ^{115}Sn). A detailed study,[10] at low bombarding energy, of the "fine structure" peaks in the tin isotopes revealed that the $1g_{9/2}$ inner-hole strengths strongly overlap in that energy range. It has also been determined that the centroid energy and the spreading width of the $1g_{9/2}$ inner-hole strength distribution increase smoothly with increasing mass number, that is, while going away from the shell closure. A transition from line fragmentation to line broadening occurs when the mass number varies from $A=112$ to $A=124$.[3–7,10]

In contrast to this abundance of experimental work, much less information has been reported on high-lying particle states. Concerning these states, we report here on an experimental investigation of the tin isotopes extending from $A=113$ to $A=125$. The $(\alpha,{}^3\mathrm{He})$ reaction has been studied at 183 MeV incident energy on ^{124,122,120,118,116,112}Sn targets. Partial results of the ^{120,118,116}Sn $(\alpha,{}^3\mathrm{He})$ reactions have been previously reported[11] and are superseded by the present paper. As shown in Ref. 11, the strong selectivity of this reaction for high-l transfer is well suited for the investigation of the single-particle response function up to high excitation energies. The pronounced structures observed in the residual energy spectra have been assigned to neutron stripping to high-spin orbitals belonging to the next major shell above the Fermi sea.

After a brief description of the experimental method (Sec. II), the results and their distorted-wave Born approximation (DWBA) analysis are presented in Secs. III and IV. Our results provide evidence on single-particle strength distributions from the neutron shell above the $N=82$ shell closure. We find that the strong cross-section concentration around 5 MeV, which constitutes a sharp peak in the heavier-isotopes spectra, arises mainly from an $l=6$ transfer. The whole cross section observed between 5 and 10 MeV excitation energy can be explained by a mixture of three l transfers, i.e., $l=3$, 5, and 6. In Sec. V the experimental spectra are compared with the predictions from the quasiparticle-phonon nuclear model. A summary and conclusions are given in Sec. VI.

II. EXPERIMENTAL PROCEDURE

The experiment was performed with an α-particle beam of 183 MeV delivered by the K 220 Orsay synchrocyclotron. The thicknesses and isotopic enrichments of the self-supporting metallic tin target foils are listed in Table I. With the beam transport system set in an achromatic mode, a current of 50–400 nA on target was measured in a Faraday cup. The outgoing particles were detected by two multiwire proportional chambers placed at the focal plane of the large magnetic spectrometer

 ©1991 The American Physical Society

TABLE I. Characteristics of the targets used in the study of the $(\alpha, {}^3\mathrm{He})$ reactions.

Isotopes	Thickness (mg/cm^2)	Enrichment (%)	Q_{value}[a] (MeV)
^{124}Sn	5.13	94.7	−14.81
^{122}Sn	5.29	90.8	−14.646
^{120}Sn	12.0	98.0	−14.397
^{118}Sn	25.0	96.6	−14.097
^{116}Sn	22.0	95.6	−13.637
^{112}Sn	1.22	80.0	−12.835

[a]Reference 25.

Montpellier.[12] Following the position detectors, two plastic scintillators (3 and 5 mm thick) were used to provide the time-of-flight and energy-loss signals necessary for a clean identification of the ^{3}He particles. The absolute cross sections were determined using the known values of the target thickness and of the spectrometer solid angle. The error in the absolute cross-section scales is estimated to be of the order of ±10%.

An excitation energy range of around 25 MeV has been explored using three successive exposures at different magnetic fields. We obtained an overall energy resolution of 100 keV with the thin ^{112,122,124}Sn targets. With the thicker ones, the energy resolution was limited to around 200 keV.

The excitation energy of the observed levels has been determined from calibration of the focal-plane detector using known energies of the low-lying states of the tin isotopes (in particular the main $1h_{11/2}$ level) and some strong states from neutron stripping reactions on ^{12}C and ^{16}O measured with a Mylar target.

For the ^{124,120,112}Sn$(\alpha, {}^3\mathrm{He})$ reactions, a complete angular distribution was measured from 2.5° to 15° (laboratory angle) in 2° steps. The ^{122,118,116}Sn$(\alpha, {}^3\mathrm{He})$ reactions were investigated at only two angles: 4° and 8°.

III. EXPERIMENTAL RESULTS

The resulting spectra from the $(\alpha, {}^3\mathrm{He})$ reaction on the tin isotopes, at a laboratory angle of 8°, are presented in Fig. 1. One observes the low-lying levels with a very strong population of the $1h_{11/2}$ main fragment, thus demonstrating the selectivity of the $(\alpha, {}^3\mathrm{He})$ process for large l values.

Beyond a few MeV excitation energy, complex structures dominate the spectra. For the heavier tin isotopes (121, 123, and 125), they consist of a sharp, strong peak at $Q \approx -20$ MeV, and a shoulder extending up to around −25 MeV Q value. A clear broadening of the whole structure is observed with decreasing mass number. This leads to a rather structureless spectrum in the case of ^{113}Sn.

The continuum part (beyond −26 MeV Q value) of the spectra does not exhibit any pronounced structure. As a first step, one could assume that the observed cross section in this region arises from the breakup of the α particle since the breakup process is known to provide an im-

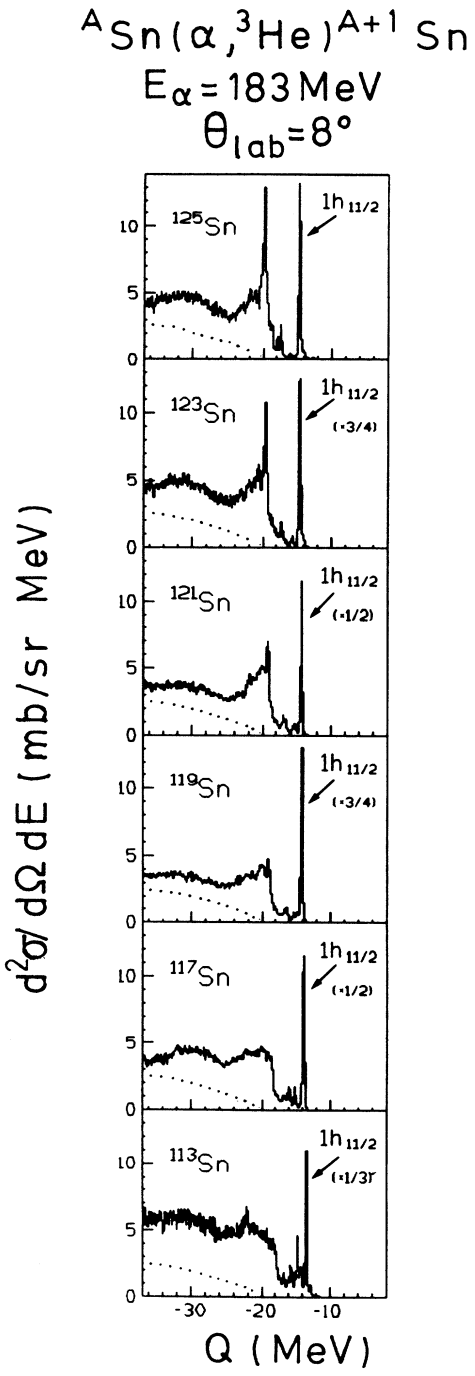

FIG. 1. ^{3}He energy spectra from the reaction $(\alpha, {}^3\mathrm{He})$ on ^{124,122,120,118,116,112}Sn targets at a laboratory angle of 8°. On the horizontal scales are plotted the Q values. The vertical scale indicates the double-differential cross sections in mb/sr MeV. Dotted lines indicate the background shape calculated with the plane-wave breakup model, normalized as mentioned in the text. Also indicated is the main $1h_{11/2}$ single-particle state with the spectroscopic properties quoted in Table III. The peak around −22 MeV Q value in the ^{113}Sn spectrum arises from ^{12}C and ^{16}O impurities present in the target.

portant contribution to the background in this excitation energy range. This assumption is supported by the weak dependence of the high-energy continuum on the atomic number of the target. Wu *et al.*[13] and Budzanowski *et al.*[14] have shown that breakup processes give an important conclusion to the reaction cross section of fast α particles scattered on heavy-weight nuclei. A simple Serber model[15,16] has been used to evaluate the elastic breakup contribution to the continuum. Due to the approximations in the model, only relative cross sections can be calculated which are then normalized to the data.

The normalization factor has been deduced by assuming that the experimental cross section observed around 30 MeV excitation energy in two tin spectra is only due to elastic breakup. The mean value of the normalization factor was then adopted for all the isotopes. The estimated error on the continuum cross section is of about $\pm 25\%$. This procedure, neglecting other components of the continuum such as inelastic breakup, provides however a first-order estimate of the shape of the background to be subtracted from the stripping spectra. The calculations are shown as dotted lines in Fig. 1. A significant amount of the cross section seems to originate from a different process. A broad structure is systematically observed between -26 and -36 MeV Q value in all the tin spectra. Its mean position is about 10 MeV above the complex structure located between 5 and 10 MeV. Similar broadening to the one mentioned for the $Q \approx -20$ MeV bump seems to occur for these concentrations of cross section when going from $A=125$ to $A=119$. On the basis of these observations, we consider that a high-spin single-particle excitation $1\hbar\omega \approx 10$ MeV above the strong onset of neutron strength may be responsible for the observed enhancements around $Q=-30$ MeV. Since in the present investigation the measured range of excitation energy was insufficient to perform a detailed analysis of the high excitation energy part of the spectrum, a further study of the $(\alpha, {}^3\mathrm{He})$ reaction covering 50 MeV excitation energy range is needed to obtain more information on the origin of these new broad bumps.

IV. DWBA ANALYSIS

The analysis has been carried out within the framework of the distorted-wave Born approximation, using the code DWUCK4.[17] The inputs for our calculations are the optical potentials in the α, ^{3}He, and n channels listed in Table II.

For the α channel, the optical parameters deduced from the elastic-scattering data on ^{208}Pb at 140 MeV and corresponding to the "deep" family were employed.[18] The exit channel (^{3}He) was described using the set of parameters from Djaloeis *et al.*[19] which were found to reproduce quite well the elastic-scattering results at 130 MeV on ^{90}Zr, ^{120}Sn, and ^{208}Pb targets. As regards the neutron form factor, a standard geometry (see Table II) and the separation energy procedure were used to calculate the bound-state form factor. In the case of levels located above the neutron threshold, the form factor was calculated using the resonance method proposed by Vincent and Fortune[17,20] included in the code DWUCK4.

The calculations were carried out within the zero-range (ZR) approximation. Exact finite-range (EFR) calculations for the same transitions using the code MARY[21] lead to nearly identical shapes for the angular distributions. Therefore ZR-DWBA calculations were performed using a ZR normalization constant $N=36$ consistent with the EFR calculations.

A. Analysis of the low excitation energy region

The comparison between the experimental data and DWBA predictions of the cross-section angular distributions of some low-lying well resolved states in ^{125,121,113}Sn are shown in Figs. 2 and 3. The angular distributions of the main $1h_{11/2}$ single-particle state in these three nuclei are shown in Fig. 2. Clearly excellent agreement is found for $l=5$ transfer.

Spectroscopic factors C^2S were determined using the relation:

TABLE II. Optical model potential parameters.[a]

Channel	V_0 (MeV)	r_0 (fm)	a_0 (fm)	W_0 (MeV)	r_0' (fm)	a_0' (fm)	V_{so} (MeV)	r_{so} (fm)	a_{so} (fm)	r_c (fm)
α	155	1.28	0.677	23.2	1.48	0.73				1.4
^{3}He	105	1.19	0.870	19.4	1.55	0.72				1.4
							Bound-state parameters[b]			
n	V_n	1.25	0.65				λ:25	1.25	0.65	

[a]Potential of the form $U(r)=-V_0 f(x)-iW_0 f(x')+V_C$, where $f(x_i)=|1+\exp[(r-r_i A^{1/3})/a_i]|^{-1}$, and V_C is the Coulomb potential of a uniform sphere.

[b]Strength (V_n) adjusted to reproduce empirical separation energies. The binding potential is of the form

$$U_n(r)=-V_n\left[f(r,r_0A^{1/3},a_0)-\frac{\lambda}{45.2}\frac{1}{r}\frac{d}{dr}f(r,r_{so}A^{1/3},a_{so})LS\right],$$

where $f(r,r_iA^{1/3},a_i)$ is the Woods-Saxon form.

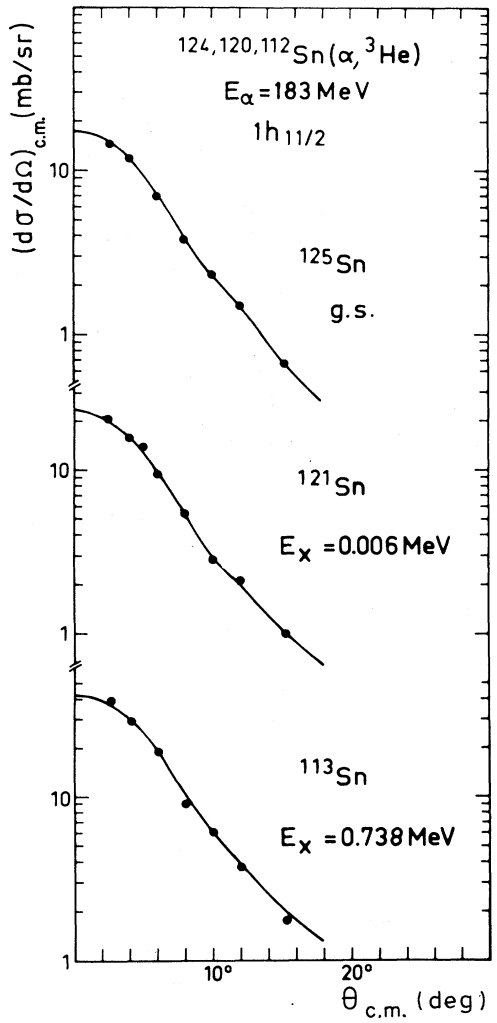

FIG. 2. Angular distributions of the main $1h_{11/2}$ state in ^{125,121,113}Sn. Solid curves are the DWBA predictions using the optical parameters listed in Table II. The deduced spectroscopic factors are quoted in Table III.

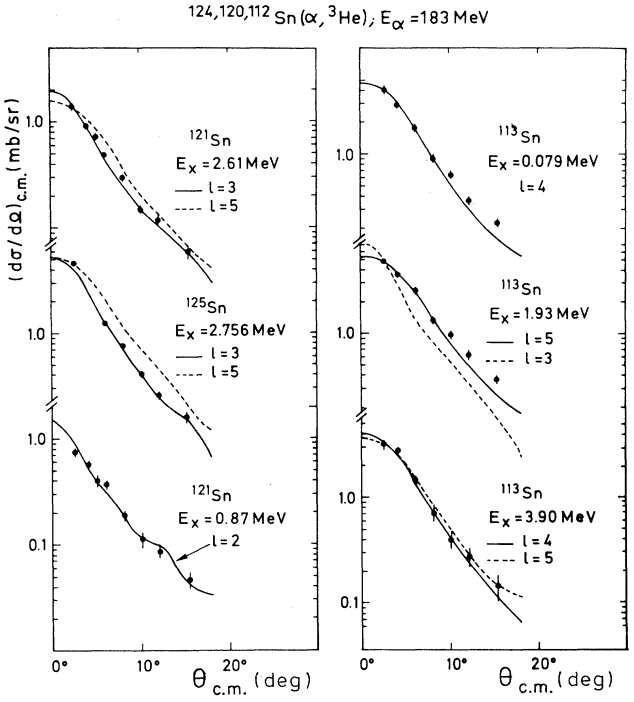

FIG. 3. Typical angular distributions of some low-lying levels in ^{125,121,113}Sn. Solid and dashed curves are the DWBA predictions for the indicated l values. Each final state is identified by its excitation energy (also indicated with arrows in Fig. 4). Vertical bars account for statistical and peak fitting errors.

$$\left[\frac{d\sigma}{d\Omega}\right]_{\text{expt}} = N\,C^2S\left[\frac{d\sigma}{d\Omega}\right]_{\text{DWBA}}$$

with $N=36$. In Table III are listed the deduced C^2S values of the main $1h_{11/2}$ component in the tin isotopes. Comparison is made with previous reported values obtained with the neutron stripping reactions, (d,p) and $(\alpha,{}^3\text{He})$, carried out at lower incident energies.[22,23] In go-

TABLE III. Spectroscopic properties of the main $1h_{11/2}$ single-particle state in the odd tin isotopes.

S_n	E_x[a] (MeV)	$(d\sigma/d\Omega)_{4^\circ}$ (mb/sr)	C^2S this work	C^2S other works (d,p)[b]	NDS adopted values[c] (d,p)	NDS adopted values[c] $(\alpha,{}^3\text{He})$
125	0	12.89	0.30		0.42	0.41
123	0	15.34	0.37		0.38	
121	0.006	16.12	0.38	0.21	0.49	
119	0.089	15.83	0.35	0.56	0.69	
117	0.314	23.59	0.50	0.81	0.79	0.62
113	0.738	29.46	0.58	1.30	1.00	

[a]NDS adopted values of the excitation energy. See Ref. 23.
[b] (d,p) reaction at 15 MeV incident energy; Ref. 22.
[c]See Ref. 23.

ing from ^{113}Sn to ^{125}Sn the C^2S values decrease, reflecting the filling of the valence $1h_{11/2}$ orbital.

Due to the limited energy resolution of this experiment, only a few well defined low-lying states were analyzed. A sample of the measured angular distributions is presented in Fig. 3. Some fragments of the $1g_{7/2}$, $2d$, $1h_{11/2}$, and $2f$ subshells are found in the low-energy region.

B. The high excitation energy region

The excitation energy range corresponding to the broad peaks (4 to 9–13 MeV) has been divided into slices, 500 KeV wide, for the three isotopes ^{125,121,113}Sn, for which complete angular distributions have been measured. A similar analysis has been carried out in the case of ^{123,119,117}Sn, where two angles (4° and 8°) were recorded. In Fig. 4 are presented the excitation energy spectra in the energy range of interest. Typical energy bins located around the 5 MeV peak are also indicated. The results of the elastic breakup calculation are shown as dotted lines in Fig. 4. The cross sections corresponding to the different energy bins have been obtained after subtraction of the calculated background.

We would like to point out that the magnitude of the subtracted background in the energy range 3–8 MeV is quite small. Therefore, the conclusions of the present analysis with regard to the l identification and the amount of strength are independent of the assumptions made to evaluate the continuum contribution.

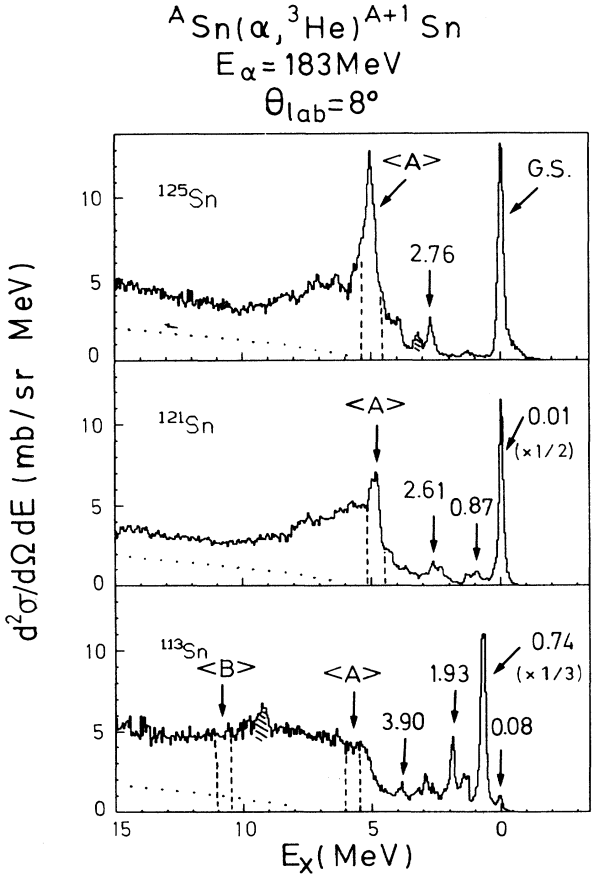

FIG. 4. ^{3}He energy spectrum from the ^{124,120,112}Sn (α, ^{3}He) reactions. The horizontal scale indicates the excitation energy in the ^{125,121,113}Sn nuclei. Hatched peaks originate from the (α, ^{3}He) reaction on ^{12}C and ^{16}O impurities present in the targets. Dotted lines show the background line shape calculated with the plane-wave breakup model. Angular distributions of the peaks and slices indicated with arrows are shown in Figs. 3 and 5.

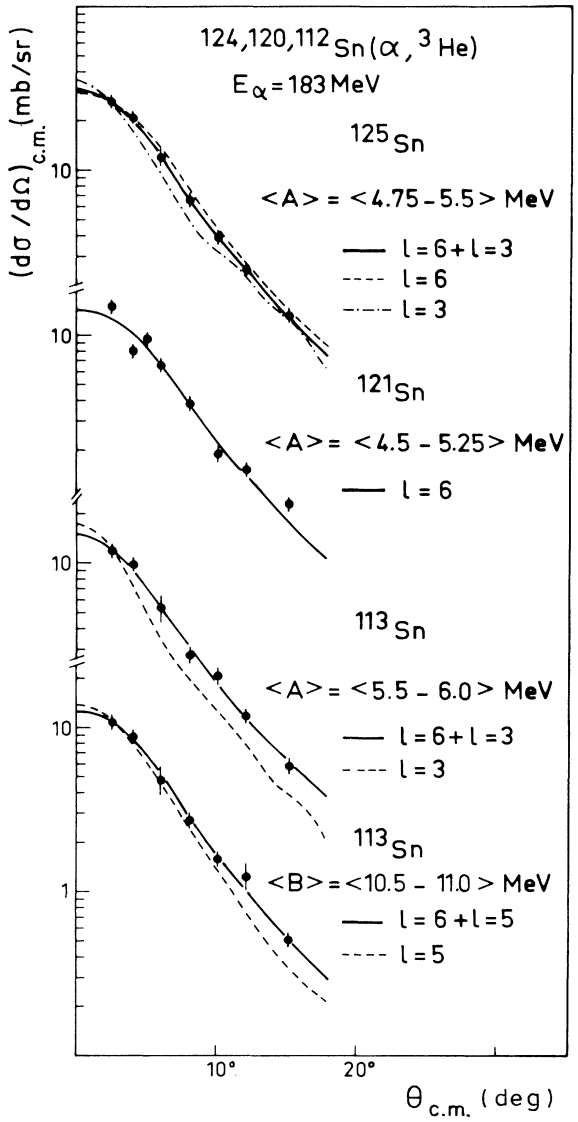

FIG. 5. Typical angular distributions of some high-lying levels in ^{125,121,113}Sn. Solid, dashed, and dash-dotted curves are the DWBA predictions for the indicated l values. Pure $l=6$ transfer is shown only when it clearly distinguishes from the multiple l transfer curve. The limits of the energy bins are listed (these bins are also indicated with arrows in Fig. 4). Vertical bars account for statistical and background estimation errors.

The angular distribution of each slice has been analyzed using two different hypotheses. A single l transfer or a weighted mixture of up to three different l values, corresponding to the subshells lying in the energy range of interest, namely, $2f$, $1h$, and $1i$. Typical angular distributions are shown in Fig. 5 where the solid lines indicate the best fits obtained using the above mentioned procedure.

The overall result of this analysis is summarized in Table IV. The sharp peak around 5 MeV in the ^{125}Sn and

TABLE IV. High-lying neutron strengths in ^{125,121,113}Sn isotopes.

Isotope	E_x (MeV)	Multiple l transfer[a] l	(nlj)	C^2S	Single l transfer[b] l	(nlj)	C^2S
^{125}Sn	|3.7–4.7|	3	$(2f_{7/2})$	0.72	3	$(2f_{7/2}$	2.96
		6	$(1i_{13/2})$	0.08	6	$(1i_{13/2})$	0.11
	$\langle A \rangle$	3	$(2f_{7/2})$	1.84	3	$(2f_{7/2})$	8.85
	|4.7–5.5|	6	$(1i_{13/2})$	0.22	6	$(1i_{13/2})$	0.26
	|5.5–6.0|	3	$(2f_{5/2})$	0.80	3	$(2f_{5/2})$	6.47
		6	$(1i_{13/2})$	0.09	6	$(1i_{13/2})$	0.10
	|6.0–7.0|	3	$(2f_{5/2})$	2.99	3	$(2f_{5/2})$	7.23
		5	$(1h_{9/2})$	0.56	5	$(1h_{9/2})$	1.12
		6	$(1i_{13/2})$	0.06	6	$(1i_{13/2})$	0.76
	|7.0–9.0|	6	$(1i_{13/2})$	0.32	5	$(1h_{9/2})$	1.86
					6	$(1i_{13/2})$	0.32
	$\sum$|3.7–9.0|	$\sum l=3$		6.35			
		$\sum l=5$		0.56			
		$\sum l=6$		0.77			
^{121}Sn	|3.8–4.5|	3	$(2f_{7/2})$	0.24	3	$(2f_{7/2})$	0.85
		6	$(1i_{13/2})$	0.03	5	$(1h_{9/2})$	0.18
					6	$(1i_{13/2})$	0.04
	$\langle A \rangle$	6	$(1i_{13/2})$	0.12	3	$(2f_{7/2})$	3.46
	|4.5–5.2|				5	$(1h_{9/2})$	0.61
					6	$(1i_{13/2})$	0.12
	|5.2–9.5|	3	$(2f_{5/2})$	5.65	3	$(2f_{5/2})$	23.63
		5	$(1h_{9/2})$	0.65	5	$(1h_{9/2})$	3.26
		6	$(1i_{13/2})$	0.39	6	$(1i_{13/2})$	0.59
	$\sum$|3.8–9.5|	$\sum l=3$		5.89			
		$\sum l=5$		0.65			
		$\sum l=6$		0.54			
^{113}Sn	|4.0–5.0|	3	$(2f_{7/2})$	0.84	3	$(2f_{7/2})$	1.10
		6	$(1i_{13/2})$	0.02	5	$(1h_{9/2})$	0.31
					6	$(1i_{13/2})$	0.06
	|5.0–5.5|	5	$(1h_{9/2})$	0.19	5	$(1h_{9/2})$	0.30
		6	$(1i_{13/2})$	0.02	6	$(1i_{13/2})$	0.06
	$\langle A \rangle$	3	$(2f_{7/2})$	0.56	3	$(2f_{7/2})$	1.88
	|5.5–6.0|	6	$(1i_{13/2})$	0.06	5	$(1h_{9/2})$	0.46
					6	$(1i_{13/2})$	0.09
	|6.0–8.5|	3	$(2f_{5/2})$	3.45	3	$(2f_{5/2})$	23.89
		6	$(1i_{13/2})$	0.39	5	$(1h_{9/2})$	2.53
					6	$(1i_{13/2})$	0.48
	|8.5–11.0|	5	$(1h_{9/2})$	0.30	5	$(1h_{9/2})$	2.68
		6	$(1i_{13/2})$	0.43	6	$(1i_{13/2})$	0.48
	|11.0–13.0|	6	$(1i_{13/2})$	0.38	5	$(1h_{9/2})$	2.24
					6	$(1i_{13/2})$	0.38
	$\sum$|4–13|	$\sum l=3$		4.85			
		$\sum l=5$		0.49			
		$\sum l=6$		1.3			

[a]Results of the analysis using an automatic fitting procedure assuming multiple l transfer for the slices located in the indicated energy range.

[b]Results of the analysis using an automatic fitting procedure assuming a unique l transfer. When no values are quoted it means that the corresponding pure l transfer would not reproduce the experimental angular distributions in that energy range.

^{121}Sn arises mainly from a $l=6$ transfer although the fits are slightly better using an additional weak component from the $l=3$ transfer (see Fig. 4 and Table IV). In all cases, the $l=6$, $1i_{13/2}$ strength spreads over the whole excitation energy range (4 to 10–13 MeV) with variable mixture of $l=3$ and $l=5$ strengths. The result of the analysis carried out with a single $l=6$ transfer shows that the sum-rule limit is reached in ^{121}Sn and even exceeded in the case of ^{125}Sn and ^{113}Sn (see Table IV). For the other l transfers ($l=5$ and $l=3$), the same conclusions can be drawn from Table IV, with values of the sum-rule limit exceeded by much larger factors (2 to 20).

Because of the lack of sensitivity of the l dependence of the angular distribution it is not possible from the analysis to unravel the neutron strength distribution of individual subshells. Moreover, the mismatch of the $(\alpha,{}^3\mathrm{He})$ reaction for low l transfer makes the C^2S values obtained for the $2f$ strength unreliable.

In conclusion, the neutron strength observed in the energy range 4–10 MeV originates mainly from the $1i_{13/2}$ orbital. As regards the neighboring subshells ($1h_{9/2}$, $2f_{7/2}$, $2f_{5/2}$), their contribution can only be inferred on the basis of sum-rule arguments.

V. COMPARISON TO THEORETICAL PREDICTIONS

Theoretical predictions for the high-lying subshells $2f_{7/2}$, $2f_{5/2}$, $1h_{9/2}$, and $1i_{13/2}$, using the quasiparticle-phonon nuclear model and the strength function method have been reported by Vdovin and Stoyanov.[24] In Fig. 6, we show the result of these calculations for the two isotopes at the limits of the range of isotopes studied. The theoretical cross sections have been obtained by the conversion of the theoretical strength functions, through DWUCK calculation, into double-differential $(\alpha,{}^3\mathrm{He})$ cross sections (mb/sr MeV). In the figure, Σ represents the sum of all the individual contributions. The calculations show that all the subshells are strongly fragmented. The total spectrum is strongly dominated by the $1i_{13/2}$ strength. The other subshells such as $1h_{9/2}$ and especially $2f$ contribute very little to the resulting spectra. This conclusion is in good agreement with the DWBA analysis presented in the previous section. The reaction $(\alpha,{}^3\mathrm{He})$ at 183 MeV appears as a very effective tool to excite preferentially the highest spin subshells available in the energy range covered by the present experiment.

The strength distributions of the subshells are predicted to be strongly overlapping. This prediction has been tested by means of the comparison made in Fig. 7 between the experimental spectrum (background subtracted) taken at 8° and the corresponding theoretical spectra. In Fig. 7, two different theoretical predictions are presented. The dotted lines represent the contribution of the $1i_{13/2}$ neutron strength whereas the cross-dashed lines show the sum of the $2f_{7/2}$, $2f_{5/2}$, $1h_{9/2}$, and $1i_{13/2}$ strengths. In both cases, the experimental strength distribution is in overall agreement with the theoretically predicted spectra. The cross-dashed curve gives a less structured spectrum in better agreement with the experimental ones.

The increasing damping when the mass number decreases from $A=125$ to $A=113$ is qualitatively reproduced by the theoretical predictions. However, the damping of these high-lying orbitals seems to be much larger than predicted. In the heavier isotopes, the second maxima of the theoretical strength distributions is not observed experimentally. In the lighter isotopes, the experimental results reveal structureless cross-section spectra while some broad peaks are theoretically predicted.

According to theoretical calculations[24] the two-humped form of the $1i_{13/2}$ strength function is a result of the strong coupling of this subshell with the lowest quadrupole vibration of the core. As in other similar cases,[1] the quasiparticle-phonon model (QPM) predicts much

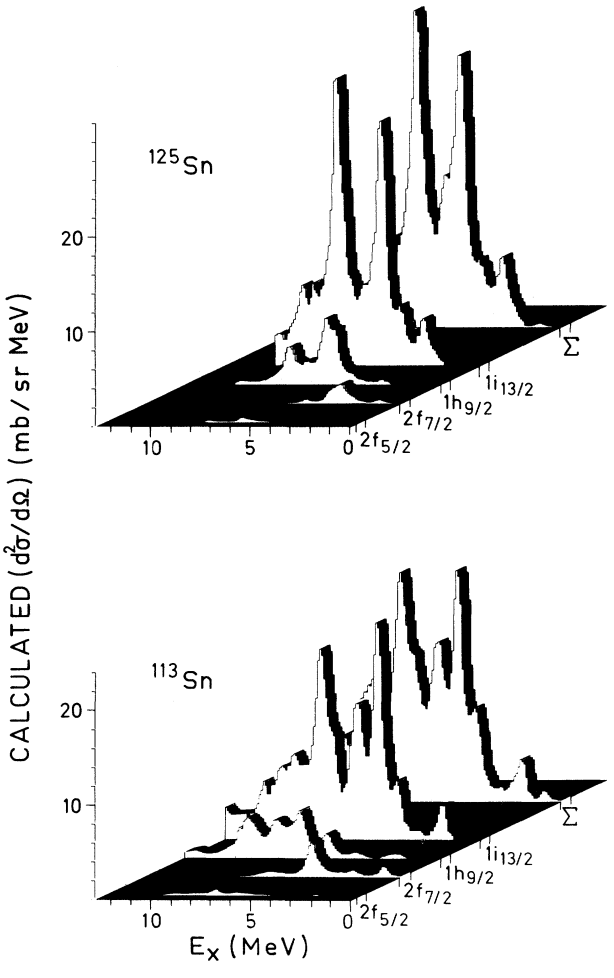

FIG. 6. Quasiparticle-phonon model predictions of the cross sections in ^{125,113}Sn obtained by the conversion of the theoretical strength functions (from Ref. 24) into double differential $(\alpha,{}^3\mathrm{He})$ cross sections. The sum of all individual contributions is represented by Σ.

more pronounced peaks in the high-energy part of the strength distribution than is seen experimentally. As was pointed out in Ref. 1, the reason for this is restricted complexity of the model wave function of the QPM. So, the dependence of the spreading width on the level density (and consequently on the excitation energy) in the QPM calculations is much weaker than in real nuclei.

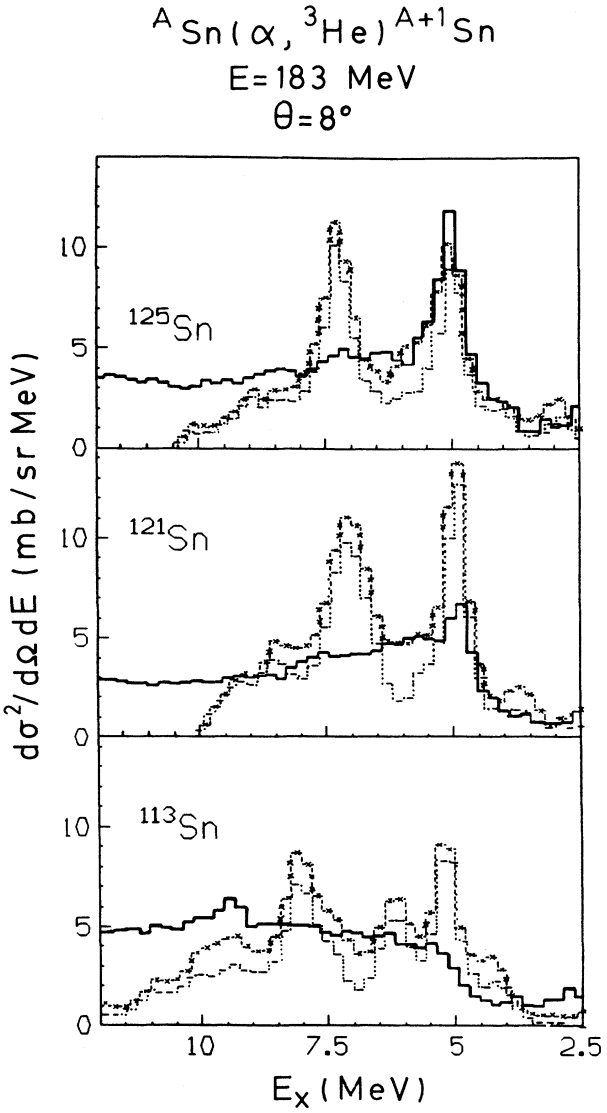

FIG. 7. Comparison between experimental (solid line) and theoretical (α,^{3}He) cross sections, at 8° laboratory angle, for ^{125,121,113}Sn in the excitation energy region of the high-lying neutron states. The dotted lines represent the calculated contribution of the $1i_{13/2}$ neutron strength. The $-\times-\times-$ histograms show the theoretical prediction taking into account the sum of the $1i_{13/2}$, $1h_{9/2}$, and $2f$ strengths.

VI. SUMMARY AND CONCLUSIONS

We have studied high-lying neutron states in the tin isotopes by means of the (α,^{3}He) reaction at 183 MeV incident energy. The large enhancement of cross section observed between 5 and 10 MeV excitation energy in the six nuclei investigated here arises from proton stripping to high-lying outer subshells and displays strong similarities with those observed in the pick-up experiments on deeply-bound neutron-hole states. Indeed, in neutron pick-up experiments, the overlapping $1g$ and $2p$ inner neutron shells appear as a complex structure with a narrow component around 5 MeV and a broader structure located in the tail of the peak.[4] A broadening of the whole structure is observed when the mass number varies from $A=112$ to $A=125$. This behavior is quite similar to the one described above the neutron particle strength on the same isotopic chain.

In both cases, the spreading of the strength distribution increases as one moves away from the corresponding shell closure (from $A=125$ to $A=112$, shell closure $N=82$ for the particle states; from $A=112$ to $A=125$, shell closure $N=50$ for the hole states).

The Dubna group has been rather successful in reproducing the empirical systematics, using the quasiparticle-phonon coupling model.[1,24] They have reached a good qualitative understanding of the damping of such nuclear excitations. In general, the centroid energies, the total amount of strength, and overlap between different subshells are in reasonable agreement with our experimental results. However, the detailed structure of the predicted strength distributions displays rather narrow concentration of strengths, in particular for the heavier tin isotopes, which are not observed experimentally. In the near future, exclusive experiments looking for the neutron decay of the high-lying states, will certainly lead to progress in the understanding of the very large spreading observed experimentally as compared to the quasiparticle-phonon predictions.

A second cross-section concentration is found between 10 and 20 MeV excitation energy that can be tentatively attributed to the stripping reaction. The experimental data suggest that $2\hbar\omega$ single-particle strengths may be responsible for these observed cross-section enhancements. Similar spreading to the one mentioned for the 5-MeV peak seems to occur for these proposed $2\hbar\omega$ excitations. Further investigation is required to confirm the origin of these new broad bumps.

ACKNOWLEDGMENTS

Professor A. I. Vdovin is kindly acknowledged for interesting comments on the manuscript. We would like to thank the operating staff of the synchrocyclotron for the smooth running of the accelerator. One of us (C.P.M.) wishes to thank Fundación Antorchas and CONICET, Argentina, as well as the IN2P3/CNRS, France, for financial support. This work was partially supported by the U.S. National Science Foundation under Grant No. PHY86-11210.

*On leave from Departamento de Física, Universidad Nacionale de La Plata, C.C. No. 67, 1900 La Plata, Argentina.
†Present address: Centre d'Etudes Nucléaires de Bordeaux-Gradignan, Le Haut Vigneau 33170 Bordeaux-Gradignan, France.
‡Present address: Institut de Physique Nucléaire, Lyon, 69622 Villeurbanne CEDEX, France.

[1]S. Galès, Ch. Stoyanov, and A. I. Vdovin, Phys. Rep. **166**, 125 (1988).
[2]M. Sakai and K. Kubo, Nucl. Phys. **A185**, 217 (1972).
[3]S. Y. Van der Werf, Phys. Rev. Lett. **33**, 712 (1974).
[4]E. Gerlic *et al.*, Phys. Lett. **57B**, 338 (1975).
[5]G. M. Crawley, in Proceedings of the International Conference on the Structure of Medium Heavy Nuclei, The Institute of Physics, Rhodos, Greece, 1979 (unpublished), p. 187; in Proceedings of the International Symposium on Highly Excited States, Osaka, Japan, 1980 (unpublished), p. 590.
[6]S. Galès, Nucl. Phys. **A354**, 193c (1981); Nukleonika **27**, 82 (1982); J. Phys. (Paris) **45**, C4-39 (1984).
[7]H. Langevin-Joliot, in Proceedings of the XIVth Masurian Summer School, Lake Mikolajki, Poland, 1983 (unpublished).
[8]H. Langevin-Joliot *et al.*, Phys. Lett. **114B**, 103 (1982).
[9]R. H. Siemssen *et al.*, Phys. Lett. **114B**, 323 (1982); R. H. Siemssen *et al.*, Nucl. Phys. **A405**, 205 (1983).
[10]E. Gerlic *et al.*, Phys. Rev. C **21**, 124 (1980).
[11]S. Galès *et al.* Phys. Lett. **144B**, 323 (1984).
[12]M. Morlet and A. Willis, Institut de Physique Nucléaire–Orsay Internal Report No. IPNO-PhN-7915, 1979; J. Guillot, Thesis, Institut de Physique Nucléaire–Orsay, 1982.
[13]J. R. Wu, C. C. Chang, and H. D. Holmgren, Phys. Rev. Lett. **40**, 1013 (1978).
[14]A. Budzanowski *et al.*, Phys. Rev. Lett. **41**, 635 (1978).
[15]R. Serber, Phys. Rev. **72**, 1008 (1947).
[16]N. Matsuoka *et al.*, Nucl. Phys. **A311**, 173 (1978).
[17]P. D. Kunz, University of Colorado, code DWUCK (unpublished).
[18]D. A. Goldberg *et al.*, Phys. Rev. C **7**, 1938 (1973).
[19]A. Djaloeis *et al.*, Nucl. Phys. **A306**, 221 (1978).
[20]C. M. Vincent and H. T. Fortune, Phys. Rev. C **2**, 782 (1970).
[21]N. S. Chant and J. N. Graig, Phys. Rev. C **14**, 1763 (1976).
[22]E. J. Schneid, A. Prakash, and B. L. Cohen, Phys. Rev. **156**, 1316 (1967).
[23]See Nucl. Data Sheets **32**, 531 (1981) for ^{125}Sn; **29**, 483 (1980) for ^{123}Sn; **26**, 423 (1979) for ^{121}Sn; **26**, 207 (1979) for ^{119}Sn; **50**, 63 (1987) for ^{117}Sn; **33**, 53 (1981) for ^{113}Sn.
[24]A. I. Vdovin and Ch. Stoyanov, Report No. JINR, E4-85-352, Dubna, 1985; A. I. Vdovin, E. M. Galinskij, and Ch. Stoyanov, Report No. JINR, P4-86-196, Dubna, 1986; Ch. Stoyanov, A. I. Vdovin, and V. V. Voronov, in Proceedings of the International School on Nuclear Physics, Alustha, U.S.S.R., 1985, edited by V. G. Soloviev and Yu. P. Popov; and private communication.
[25]C. Maples, G. W. Goth, and J. Cerny, Nucl. Data Tables A **2**, 429 (1966).